Analysis of the recent trends in vegetation dynamics and its relationship with climatological factors using remote sensing data for Caspian Sea watersheds in Iran

Iman Rousta[1,3]*, Mohammad Mansourmoghaddam[1,2] , Haraldur Olafsson[3], Jaromir Krzyszczak[4] ,
Piotr Baranowski[4] , Hao Zhang[5], and Przemysław Tkaczyk[6]

[1]Department of Geography, Yazd University, Yazd 8915818411, Iran
[2]Department of Remote Sensing, Yazd University, Yazd 8915818411, Iran
[3]Department of Physics, Institute for Atmospheric Sciences-Weather and Climate, University of Iceland and Icelandic Meteorological Office (IMO), Bustadavegur 7, IS-108 Reykjavik, Iceland
[4]Institute of Agrophysics, Polish Academy of Sciences, Doświadczalna 4, 20-290 Lublin, Poland
[5]Department of Environmental Science and Engineering Jiangwan campus, Fudan University, 2005 Songhu Road, Yangpu District Shanghai 200438, China
[6]Department of Agricultural and Environmental Chemistry, University of Life Sciences in Lublin, Akademicka 15, 20-950 Lublin, Poland

Abstract. This study used NDVI, ET, and LST satellite images collected by moderate resolution imaging spectroradiometer and tropical rainfall measuring mission sensors to investigate seasonal and yearly vegetation dynamics, and also the influence of climatological factors on it, in the area of the Caspian Sea Watersheds for 2001-2019. The relationships have been assessed using regression analysis and by calculating the anomalies. The results showed that in the winter there is a positive significant correlation between NDVI and ET, and also LST (R = 0.46 and 0.55, p-value = 0.05, respectively). In this season, the impact of precipitation on vegetation coverage should not be significant when LST is low, as was observed in the analysed case. In spring, the correlation between NDVI and ET and precipitation is positive and significant (R = 0.86 and 0.55, p-value = 0.05). In this season, the main factor controlling vegetation dynamics is precipitation, and LST's impact on vegetation coverage may be omitted when precipitation is much higher than usual. In the summer, the correlation between NDVI and ET is positive and significant (R = 0.70, p-value = 0.05), while the correlation between NDVI and LST is negative and significant (R = –0.45, p-value = 0.05). In this season, the main factor that controls vegetation coverage is LST. In the summer season, when precipitation is much higher than average, the impact of LST on vegetation growth is more pronounced. Also, higher than usual precipitation in the autumn is the reason for extended vegetation coverage in this season, which is mainly due to increased soil moisture.

Keywords: Caspian Sea watersheds, evapotranspiration, tropical rainfall measuring mission, normalized difference vegetation index, land surface temperature

INTRODUCTION

Climate change affects the Earth's ecosystems to a significant extent, but not every region is impacted by it in the same manner. It is and will be more pronounced for regions characterized by a sensitive equilibrium between the local ecosystem and climate, like parts of the Mediterranean or the Sahelian regions (Lereboullet *et al*., 2013; Fayech and Tarhouni, 2020; Picoli *et al.,* 2019; Rousta *et al.,* 2021; Shahbazi *et al.,* 2009). Vegetation is a very sensitive part of human life and activity and is susceptible to climate change impacts on the environment. On the other hand, vegetation also influences climate change, as to mitigate and adapt to climate change new ways to cultivate vegetation are being sought, *e.g.* zero tillage (Vilček *et al.,* 2019). The total amount of vegetation and the length of the growing season are known as vegetation dynamics when considered in unison, and both of these components are susceptible to changes in climate (Bagherzadeh *et al.,* 2020; Zhang 2020). There is a close relationship between climatic factors and vegetation coverage (Rousta *et al.,* 2020a; Rousta *et al.,* 2020b; Chen *et al.,* 2022). Vegetation cover is often used as a climate impact indicator in climate change studies. Also, because of the vital role of vegetation changes in the hydrological and

*Corresponding authors e-mail: irousta@yazd.ac.ir

biochemical cycles of the climate and its influence on the atmospheric energy balance, it must be considered in such studies (Olafsson and Rousta, 2021; Lan *et al.*, 2021).

Evapotranspiration (ET) is a crucial part of the water and energy equilibrium in the soil-plant-atmosphere system, and it is the main reason for the loss of about 60% of ground rainfall (Oki and Kanae, 2006; Paraskevas *et al.*, 2013; Miao *et al.*, 2022). ET accounts for the largest water consumption on the globe through agricultural water usage. One of the important research difficulties lies in the interannual variability of ET, which makes it challenging to explore because (1) as a process ET is too complex to be exactly predicted or measured (Brutsaert and Stricker, 1979), and (2) at the catchment scale, despite it being an intricate process and its relationships with other processes occurring in the soil-plant-atmosphere system, it has been proven that available water and energy are the main factors controlling the mean value of annual ET (Cheng *et al.*, 2011; Chao *et al.*, 2021). Zhan *et al.*, (2019) have suggested that significant biases may be caused as a result of neglecting the influence of changes in surface water area (Zhan *et al.*, 2019). Furthermore, rainfall is one of the most important factors affecting vegetation cover in different areas, which significantly affects the life of living organisms, plants in particular (Rousta *et al.*, 2018; Rousta *et al.*, 2017; Hadian *et al.*, 2014; Telak *et al.*, 2021; Zhang *et al.*, 2019c) Therefore, in the study of changes in vegetation, precipitation-related calculations are inevitably involved.

Remote sensing constitutes a comprehensive, rapid and effective method for observing certain natural processes by presenting the land surface data on a macro-scale, which reveals dynamic variation (Zhang *et al.*, 2001). Remote sensing data has become the main way in which to study both long-term and large-scale phenomena, and the major method used to obtain an overview of vegetation cover (Shen and Wang, 2001). Remote sensing has become one of the fundamental branches of science, as it enables the gathering of diversified information concerning both objects and phenomena occurring in the environment through the use of various sensors (Gu *et al.*, 2007). The technique helps to sketch out the contextual drought scenarios (Zhao X. *et al.*, 2021) not only in the spatial but also in the temporal domain. The Normalized Difference Vegetation Index (NDVI) is one of the most extensively applied remotely sensed surface indices. It is an index used to analyse a plant's growth status, spatial density dynamics, and also its phenology (Zhong *et al.*, 2010; Mansourmoghaddam *et al.*, 2021; Mansourmoghaddam *et al.*, 2022b). NDVI is an index which is very commonly used to investigate the status of vegetation. In order to measure NDVI factors such as the leaf area index (LAI) and the production pattern (Dutta *et al.*, 2015), which is based on vegetation class, land use/land cover changes (Fonge *et al.*, 2019), water stress, vegetation phenology, continental land cover mapping, and chlorophyll content

(Geerken *et al.*, 2005; Martínez and Gilabert, 2009; Moulin *et al.*, 1997; Dhar *et al.*, 2020; Mansourmoghaddam *et al.*, 2022a) are usually used. In recent times, satellite data have been more and more often used to link vegetation indices to climatic elements (Roerink *et al.*, 2003; Jelínek *et al.*, 2020). Since the 1980s, the correlations between NDVI and climate parameters in various geographic regions and ecosystems have been studied by many researchers. Tang *et al.* (2012) examined the effects of leaf area index (LAI) on ET for western Mexico during monsoon by using moderate resolution imaging spectroradiometer (MODIS) space-borne data. They found that the LAI explains about 30% of ET variability in the continental interior and 10% in the Sierra Madre Occidental. Also, they proved that ET estimated using variable infiltration capacity (VIC), which in turn was based on interannual LAI fluctuations, varied considerably at the start of the greening and dormancy phases. Additionally, it was observed that at the beginning of the monsoon season that ET was influenced by the start of the greening phase, which indicates that the observation of the LAI anomalies may be beneficial in the forecasting of ET values early in the season (Tang *et al.*, 2012). In the research of Alemu *et al.* (2014), a thermal-based simplified surface energy balance operational (SSEBOp) ET, together with NDVI calculated from MODIS Terrestrial (MOD16), and precipitation obtained from the tropical rainfall measuring mission (TRMM) were assessed for the Nile Basin for 2002-2011. Alemu *et al.* (2014) showed that negative ET anomalies were observed for seven years (including 2009 being the driest year) in >50% of the Nile Basin area, while the remaining three years (including 2007 being the wettest year) >60% of the area exhibited positive ET anomalies. They showed that a higher correlation of vegetation and monthly ET is obtained when ET calculations are based on the NDVI (R>0.77, p<0.001) rather than on thermal properties (0.52<R<0.73, p<0.001). These two different ET estimation methods gave very similar results for rainfed croplands (with thermal-based ET giving values which were higher by about 60 mm y^{-1}) while for the wetlands the results were significantly divergent (thermal-based ET being 440 mm y^{-1} higher than the NDVI-based one). A positive correlation between precipitation and the anomalies of thermal-based ET was observed (R = 0.6, p<0.05) for four of the nine analysed climatic zones. (Alemu *et al.*, 2014) also proved that the trends of ET were statistically significant for just about 5% of the Nile Basin.

The southern watersheds of the Caspian Sea are home to one of the greenest and most dense forests in Iran (Poorzady and Bakhtiari, 2009). Studies concerning the changes in this area are of high importance, because they are occurring rapidly, and both urban and rural areas are expanding despite the primary role of this watershed in maintaining biology and hydrology resources. The changes in the world's climate in recent decades have also added to the importance of this study. This paper attempts to find correlations between

Table 1. The characteristics of the studied watersheds in the Caspian Sea Watershed including Lahijan-Noor Watershed (LNW), Haraz-Neka Watershed (HNW), Ghareso-Gorgan Watershed (GGW) and Atrak Watershed (AW) together with their land surface temperature (LST)

Name	Area (km^2)	Elevation (m)					Average	
		Maximum	Minimum	Average	Majority	Minority	Precipitation (mm)	LST (°C)
LNW	11000	4644	–28	1365	1	–27	856.7	17.89
HNW	18800	5587	–28	1316	–28	355	541.2	19.79
GGW	13200	3456	–29	771	1	–29	377.2	23.81
AW	27000	2896	–30	990	1	–30	321.3	26.87

vegetation dynamics and climatological factors in the Caspian Sea Watersheds (CSW) area. The relationship between vegetation dynamics and climatological factors is assessed by employing NDVI, ET, LST and precipitation derived from MODIS and TRMM datasets. This study focuses on (a) investigating vegetation coverage changes over the CSW, (b) analyzing the time-series of MODIS-derived NDVI, ET and LST, and TRMM-derived precipitation, (c) assessing the relationship between NDVI and ET, LST and precipitation over the CSW.

MATERIAL AND METHODS

The research area studied is the Caspian Sea Watershed (CSW) located in the north of Iran. The study area is located between 35 and 38°N and 49 and 58°E. The total area is about 70000 km^2, and it contains four main watersheds, including the Lahijan-Noor Watershed (LNW), Haraz-Neka Watershed (HNW), Ghareso-Gorgan Watershed (GGW), and Atrak Watershed (AW) having an area of approx. 11000, 18800, 13200, and 27000 km^2, respectively. The highest elevation in the study area is about 5587 m in HNW, and the lowest elevation is about –30 m in AW. The highest amount of precipitation in the CSW area is in LNW, and its lowest
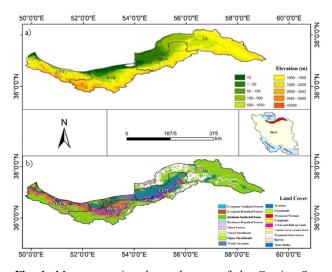
is in the AW watershed (856.7 and 321.3 mm, respectively). LST in the CSW area varies from 17.89 to 26°C in the AW and LNW watersheds, respectively (Fig. 1 and Table 1) also, there is a significant difference between the land cover of each sub-basins of CSW (Table 2).

The current study makes use of 1579 satellite images. The first dataset consisted of 437 MODIS NDVI, 874 ET as well as 228 TRMM precipitation images for the period from 2001 to 2019 with a 0.1-degree resolution, and 40 shuttle radar topography mission (SRTM) digital elevation images with a resolution of 1 arc-second (~30 m), which were used to provide an elevation map of the study area (Zandbergen 2008). The second dataset consisted of indices derived from the first dataset, including the Z score (anomaly) of NDVI, ET, and TRMM precipitation.

The calculation of NDVI takes into account that in healthy leaves (that is, the green ones) near-infrared (NIR) radiation is highly reflected by the mesophyll, while a huge ratio of the radiation in the red visible (RED) band is assimilated by the chlorophyll and other pigments (Tavazohi and

Fig. 1. Maps presenting the study area of the Caspian Sea Watershed including Lahijan-Noor Watershed (LNW), Haraz-Neka Watershed (HNW), Ghareso-Gorgan Watershed (GGW) and Atrak Watershed (AW), and an elevation profile (a) and land cover types from MODerate resolution Imaging Spectroradiometer (MODIS) MCD12Q1 image from 2017 (b).

Table 2. Land cover types of Caspian Sea Watershed including Lahijan-Noor Watershed (LNW), Haraz-Neka Watershed (HNW), Ghareso-Gorgan Watershed (GGW) and Atrak Watershed (AW) together with their area (km^2) from MODerate resolution imaging spectroradiometer (MODIS_ MCD12Q1 images using the International Geosphere-Biosphere Programme (IGBP) classification (Didan *et al.*, 2015; Loveland *et al.*, 1999)

Land cover type	LNW	HNW	GGW	AW
Evergreen needleleaf forests	2	2	8	0
Evergreen broadleaf forests	22	0	0	0
Deciduous needleleaf forests	0	0	0	0
Deciduous broadleaf forests	2386	2263	444	0
Mmixed forests	869	1039	1161	0
Closed shrublands	0	0	0	0
Open shrublands	11	359	1358	6490
Woody savannas	1196	1563	913	0
Savannas	833	1452	116	0
Grasslands	5156	8648	3104	17624
Permanent wetlands	82	63	2	2
Croplands	169	2169	5722	1822
Urban and built-up lands	170	511	185	53
Cropland/natural vegetation mosaics	7	89	19	0
Permanent snow and ice	0	0	0	0
Barren	92	141	146	959
Water bodies	5	500	23	51
Total	11000	18800	13200	27000

Nadoushan, 2018). This situation is reversed in the case of unhealthy or water-stressed vegetation (Chanklan *et al.,* 2017; Dutta *et al.,* 2015; Ghafarian Malamiri *et al.,* 2018; Quaye-Ballard *et al.,* 2020). NDVI is calculated as:

$$NDVI = \frac{NIR - RED}{NIR + RED}, \qquad (1)$$

where: NIR stands for near-infrared radiation (about 0.841-0.876 μm) and RED stands for radiation from the visible red band (about 0.62-0.67 μm). The NDVI variability ranges from –1 to +1, with healthy vegetation having values between 0.2 and 0.8 (Chuvieco *et al.,* 2004; Goward *et al.,* 1991; Cai *et al.,* 2014).

The NDVI index used in the presented paper was obtained from the National Aeronautics and Space Administration (NASA) Earth Observing System (EOS), specifically from the Terra- Moderate Resolution Imaging Spectroradiometer (MODIS). In order to download NDVI data for the period from 2001 to 2019 the Application for Extracting and Exploring Analysis Ready Samples (AρρEEARS) an application platform was used (https://lpdaacsvc.cr.usgs. gov.appeears) (Didan, 2015). The obtained MOD13A1 Vegetation Indices are characterized by a spatial resolution of 250 m and are shown as a composite with a 16-day interval (MOD13Q1.006_250m_16_days_NDVI). For all of the downloaded images, quality assessment (QA) was performed using the VI quality indicator (Didan *et al.,* 2015). In order to perform temporal aggregation, downloaded images were labeled by ascending numbers for each year. The data was aggregated to seasonal and yearly values. Yearly NDVI was obtained by calculating the arithmetic mean from all of the 23 images for each pixel, while for the seasonal values only a subset of the data was taken into account (winter vegetation coverage for each pixel was obtained by calculating the arithmetic mean from the images labeled numerically from 1 to 6, spring vegetation coverage used images labeled from 7-12, summer vegetation coverage – 13-18, and fall vegetation coverage – 19-23):

$$Yearly \ NDVI = \frac{\sum_{i=1}^{K} NDVI_i}{K}, \qquad (2)$$

$$Winter \ NDVI = \frac{\sum_{i=1}^{6} NDVI_i}{6}, \qquad (3)$$

$$Spring \ NDVI = \frac{\sum_{i=7}^{12} NDVI_i}{6}, \qquad (4)$$

$$Summer \ NDVI = \frac{\sum_{i=13}^{18} NDVI_i}{6}, \qquad (5)$$

$$Fall \ NDVI = \frac{\sum_{i=19}^{23} NDVI_i}{5}, \qquad (6)$$

where: *i* is the index for chronologically labelling the images for each year and *K* stands for the number of images for each year (*K* = 23).

In order to calculate vegetation coverage only the pixels classified as vegetation (NDVI>0.2) were taken into account. After the summation of pixels classified as representing vegetation was performed, the result was multiplied by the size of one pixel (0.625 km^2). After that, the ARC GIS cell

statistics were used to obtain several statistical indicators, such as NDVIs means and standard deviations (both yearly, and for each season). They were also calculated both for the individual CSW sub-basins and for individual years from the analysed period spanning from 2001 to 2019. Additionally, the means for the entire period were calculated.

The current study used 874 images of the MOD16A2GF Version 6, an 8-day composite Evapotranspiration (ET-500m) product downloaded using AρρEEARS for 2001-2019. Each image from the MOD16A2GF has a spatial resolution of 500 m and is a gap-filled 8-day composite. It estimates the evapotranspiration by using the Penman-Monteith equation, for the calculation of which, the daily meteorological data from reanalyses are combined with remotely sensed data products, such as vegetation dynamics, albedo, or land cover obtained from MODIS (Running *et al.,* 2019).

When the whole yearly set of 8-day MOD15A2H becomes available, the data is gap-filled, and the inputs are checked using the Quality Control (QC) label for each pixel using such measures as the 8-day Leaf Area Index and the Fraction of Photosynthetically Active Radiation (LAI/FPAR). If it occurs that one of the LAI/FPAR pixels fails to pass quality screening, its value is calculated by linear interpolation. After that, the enhanced MOD16 MOD16A2GF product is calculated. The MOD16A2GF ET product unit is kg m^{-2} 8 d^{-1} (8-day total ET), the scale factor is 0.1, and the valid range is from 32 767 to ~32 760. In the MOD16A2GF images, seven filling values for non-vegetated pixels are provided. They are labelled as 32 767 = filled value, 32 766 = land cover (LC) identified as perennial salt or water bodies, 32 765 = LC meaning barren land or very sparse vegetation (rock, tundra, desert), 32 764 = LC assigned as perennial snow or ice, 32 763 = LC meaning "permanent" wetlands or inundated marshland, 32 762 = land cover assigned as urban or built-up land, 32 761 = land cover that is "unclassified". The seasonal and yearly arithmetic mean of ET was determined for each pixel using:

$$Yearly \ ET = \frac{\sum_{i=1}^{46} ET_i}{46}, \qquad (7)$$

$$Winter \ ET = \frac{\sum_{i=1}^{12} ET_i}{12}, \qquad (8)$$

$$Spring \ ET = \frac{\sum_{i=13}^{24} ET_i}{12}, \qquad (9)$$

$$Summer \ ET = \frac{\sum_{i=25}^{36} ET_i}{12}, \qquad (10)$$

$$Fall \ ET = \frac{\sum_{i=37}^{46} ET_i}{10}, \qquad (11)$$

where: index *i* was used for labelling the downloaded images in ascending order chronologically by acquisition dates.

To estimate the daytime LST, the 874 images from MOD11A2 were used. MOD11A2 is an 8-day LST that is derived by making a composition from 2 to 8 days of the MOD11A1 images (MOD11A2.006 LST Day 1km). Similarly as for NDVI or ET, the LST data for the period from 2001 to 2018 was downloaded using the Application for Extracting and Exploring Analysis Ready Samples (AρρEEARS) from

the application platform (https://lpdaacsvc.cr.usgs.gov. appeears) (Didan, 2015). The seasonal and yearly arithmetic mean of LST was determined for each pixel using:

$$Yearly\ LST = \frac{\sum_{i=1}^{46} LST_i}{46} \quad , \quad (12)$$

$$Winter\ LST = \frac{\sum_{i=1}^{12} LST_i}{12} \quad , \quad (13)$$

$$Spring\ LST = \frac{\sum_{i=13}^{24} LST_i}{12} \quad , \quad (14)$$

$$Summer\ LST = \frac{\sum_{i=25}^{36} LST_i}{12} \quad , \quad (15)$$

$$Fall\ LST = \frac{\sum_{i=37}^{46} LST_i}{10} \quad , \quad (16)$$

where: index i was used for labelling downloaded images in ascending order by acquisition dates. Before any calculations the units in the LST images were converted to °C by (Wan *et al.,* 2015):

$$LST(°C) = DN(K)0.02 - 273.15 \ , \quad (17)$$

where: *DN* stands for digital number included in the original MOD11A2 images (Kelvins), and 0.02 is a conversion coefficient (scale factor).

The 228 TIF images from the GPM_3IMERGM monthly precipitation dataset with a spatial resolution of 0.1×0.1 degree were downloaded to provide the details concerning precipitation characteristics. The unit of precipitation in the downloaded images was mm/hour, and afterwards it was converted to mm/month by multiplying the value for each pixel by the number of hours and days in each month, yearly (from January to December) and also the seasonal (winter (DJF), spring (MAM), summer (JJA) and fall (SON)) sums of precipitation were calculated (Huffman *et al.,* 2019).

An anomaly (Patel *et al.,* 2007) is calculated using the same formula as in the case of the Z-score:

$$Z_{ij} = \frac{X_{ij} - U_{ij}}{\sigma_{ij}} \ , \quad (18)$$

where: Z_{ij} is the anomaly of the ith image at the jth time-scale, X_{ij} is the parameter (such as NDVI, ET, LST, or precipitation) sum for the ith image at the jth time-scale, while U_{ij} and σ_{ij} are the long-term mean and standard deviation connected with the ith image at the jth time-scale. The anomaly is an indicator calculated for selected periods and shows how the given parameter obtained for a particular period matches the value obtained for the entire record (Patel *et al.,* 2007; Rousta *et al.,* 2020a).

The correlations between the assessed quantities were obtained by employing a linear regression with a p-value equal to 0.05. In this method, the relationship between two variables is assumed to be linear, with one variable being explanatory, whereas the other one is a dependent variable (Song *et al.,* 2005). A linear regression model is defined as:

$$y_i = a + bx_i \quad , \quad (19)$$

where: *a* and *b* are coefficients of the equation. These coefficients may be derived from the relationship between certain pairs of explanatory and dependent variables (x_{ij}, y_{ij}).
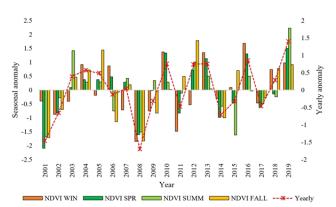

Fig. 2. Time series of yearly/seasonal (winter (WIN), spring (SPR), summer (SUMM), and fall (FALL)) normalized difference vegetation index (NDVI) anomalies in the study area during 2001-2019.

A statistical method that allows for the assessment of the relationship between a single dependent variable and several independent variables is known as a multiple regression. In a multiple regression, the independent variables have their weights, which is a measure of their relative contribution to the prediction:

$$y_i = a_0 + a_1 x_i^1 + a_2 x_i^2 + \cdots + a_n x_i^n \ , \quad (20)$$

where: y_i is the dependent variable, and $x_i^1 \cdots x_i^n$ are the explanatory variables. The weights $a_1 \ldots a_n$ were calculated using the least squares from the ANOVA package.

RESULTS

Figure 2 presents the seasonal NDVI variations in CSW for 2001-2019. The spring season is the greenest one in the study area with 53 110 km² of vegetation covering the studied area (75.82% of the whole study area), while the summer season is the second greenest season with vegetation coverage equal to 39 248 km² (56% of the whole study area). In the winter and fall seasons, about 48% of the whole study area is covered by vegetation (Fig. 2).

The two most dry (least green) winters occurred in 2008 and 2011, with a standard deviation reduced by the value of 1.85 and 1.48 compared to the overall average. The years 2016, 2010, and 2013 were the greenest, and the standard deviation was higher by the value of 1.68, 1.37, and 1.35, respectively. In the spring season, the years 2001 and 2008 were the driest, with the standard deviation being lower by the value of 2.10 and 1.60, and the years 2019 and 2010 were the greenest years, respectively, with the standard deviation increasing by the value of 1.50 and 1.33. In the summer season, the years of 2001, 2015 and 2008 were the driest with the standard deviation lower by 1.67, 1.62, and 1.51 compared to average, and the years 2019 and 2003 were the greenest with the standard deviation higher by a value of 2.23 and 1.41. In the fall season, the driest years were 2008 and 2001, with the standard deviation reduced
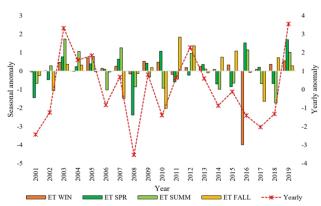
Fig. 3. Time series of yearly/seasonal (winter (WIN), spring (SPR), summer (SUMM), and fall (FALL)) evapotranspiration (ET) anomalies in the study area during 2001-2019.
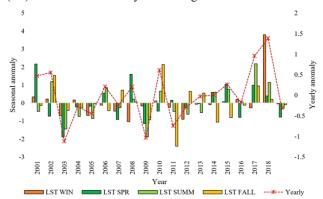

Fig. 4. Time series of yearly/seasonal (winter (WIN), spring (SPR), summer (SUMM), and fall (FALL)) land surface temperature (LST) anomalies in the study area during 2001-2019.
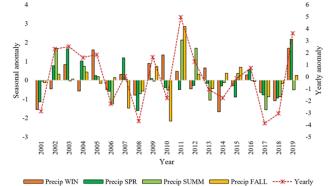

Fig. 5. Time series of yearly/seasonal (winter (WIN), spring (SPR), summer (SUMM), and fall (FALL)) precipitation (Precip) anomalies in the study area during 2001-2019.

by the value of 0.89 and 0.85, and the years 2005 and 2012 were the greenest, with the standard deviation higher by the value of 1.44 and 1.78 (Fig. 2).

During the study period, all seasons of the years 2001, 2002, 2008, 2014, and 2017 experienced a negative NDVI anomaly, with the situation in the years 2001 and 2008 being more severe than in other years. On the other hand, the years 2010, 2012, 2013, 2016, and 2019 were the years with the most positive anomaly, with the most positive anomaly occurring in 2019 as compared to the other years.

In summary, the years 2008 and 2001 with vegetation covering about 33 587 and 34 323 km^2 (47.9 and 49% of the whole study area, respectively) had the least coverage, and the years 2016 and 2019 with 43 572 and 45 196 km^2 (62.2 and 64.5% of the whole study area, respectively) had the highest vegetation coverage during the studied period of 2001-2019 (Fig. 2).

During the study period, the lowest ET in the winter period was observed in 2016 with the standard deviation lower by the value of 4 compared to the average, whereas in the other years winters had normal values of ET. In the spring season, 2001 and 2008 were the years with the lowest ET, with standard deviation values lower by a value of 1.45 and 2.39, while 2019, 2016, and 2010 were the years with the highest ET, with standard deviation values higher by the value of 1.7, 1.52, and 1.1. In the summer season 2006 and 2018, the lowest ET was observed, with standard deviation values lower by 1.03 and 1.74, and 2003 and 2007 were the years with the highest ET, with standard deviation values higher by 1.74 and 1.25. In the fall season, 2010 and 2017 had the lowest ET, with standard deviation values lower by 2.02 and 1.64, while 2005 and 2012 were the years with the highest ET, with standard deviation values higher by 1.83 and 1.37 (Fig. 3). From Fig. 3, it is evident that 2019 and 2003 were the years with the highest ET anomalies (with standard deviation values higher by 3.54 and 3.3, respectively), and 2008, 2001 and 2017 with standard deviation values lower by 3.54, 2.44, and 2.04, were the years with the lowest ET anomalies during the study period of 2001-2019 (Fig. 3).

During the 2001-2019 study period, 2008 and 2012 had the coldest winter, with an LST anomaly lower by the value of 1.04 and 0.91 compared to the average, and the year 2018 had the warmest winter, with the standard deviation higher by 3.8. In the spring season, 2003 and 2009 were the coldest years (with the standard deviation values lower by 1.9 and 1.14, respectively), while 2001 and 2008 with standard deviation values higher by 2.16 and 1.6 had the warmest spring. In the summer season, 2001 and 2019 had the coldest summer with standard deviation values lower by 1.45 and 1.9, while 2002 and 2017 had the warmest summers with standard deviation values higher by 1.18 and 2.18. In the fall season, 2011 and 2014 had the coldest falls, with standard deviation values being lower by 2.4 and 1.08 than usual, and 2002 and 2010 had the warmest falls, with standard deviation values higher by 1.53 and 2.14 (Fig. 4). From Fig. 4, it follows that during the studied period (2001-2019), 2003 and 2009 were the coldest years (with an LST anomaly of –1.12 and –1.03, respectively), and 2019 with an LST anomaly of 1.4 was the warmest (Fig. 4).

In Fig. 5, the yearly/seasonal anomalies of precipitation in the study area during 2001-2019 are presented. From these results, it may be stated that 2001 and 2014 had the driest (with the least precipitation) winters with a precipitation anomaly lower by the value of 1.55 and 1.67, and 2005, 2010 and 2019 were the wettest (with the highest
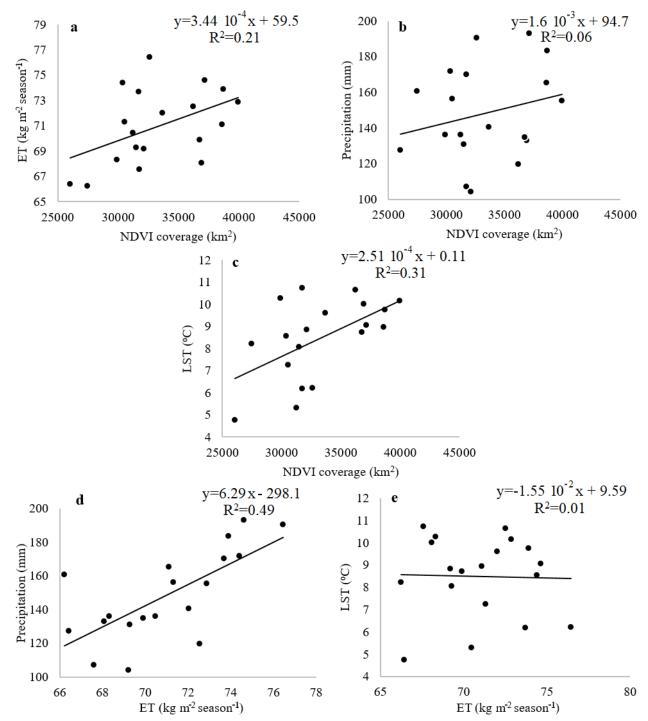
Fig. 6. The relationship between winter Normalized Difference Vegetation Index (NDVI) variations and winter Evapotranspiration (ET) (a), precipitation (b), and Land Surface Temperature (LST) (c) and the relationship between winter ET and precipitation (d), and LST (e) in Caspian Sea Watershed during 2001-2019.

precipitation) winters, with the standard deviation higher by the value of 1.6, 1.3 and 1.7. In the spring seasons, 2001 and 2008 were the driest years (with standard deviation values lower by the value of 1.14 and 1.61), while 2003, 2007 and 2019 had standard deviation values higher by the value of 1.66, 1.17, and 2.16 and had the wettest springs during the studied period (2001-2019). In the summer season of

2006 and 2017, the driest conditions were observed, with standard deviation values lower by the value of 1.27 and 1, and 2002, 2011 and 2012 had the wettest summers with standard deviation values higher by the value of 1.69, 2.13 and 10.69 In the fall season of the years 2007 and 2010 the driest conditions occurred, with standard deviation values being lower by the value of 1.47 and –2.17, while 2011 with

Table 3. The relationship between vegetation coverage (VC) variations and winter and spring Evapotranspiration (ET), precipitation and Land Surface Temperature (LST) in the Caspian Sea Watershed during 2001-2019

Year	Vegetation coverage (km²)		ET (kg m⁻² season⁻¹)		Precipitation (mm)		LST (°C)	
	Winter	Spring	Winter	Spring	Winter	Spring	Winter	Spring
2001	31753	42371	67.6	104.9	107.3	90.3	10.7	28.8
2002	29887	48917	68.3	116.6	136.3	174.3	10.3	24.1
2003	31731	53558	73.7	131.6	170.2	213.8	6.2	22.2
2004	36931	55044	68.1	125.1	133.1	185.9	10.0	24.9
2005	32597	55023	76.5	127.0	190.5	151.4	6.2	25.0
2006	36761	55527	69.9	123.5	134.9	114.8	8.7	26.2
2007	30533	54558	71.3	130.1	156.3	192.7	7.3	23.8
2008	26040	44912	66.4	93.6	127.5	69.8	4.8	27.9
2009	30371	53064	74.4	127.5	171.8	144.6	8.5	23.4
2010	38716	59913	73.9	135.3	183.4	123.0	9.8	24.5
2011	27491	48875	66.2	115.2	160.7	118.8	8.2	25.5
2012	31249	56772	70.5	119.6	136.3	128.2	5.3	24.9
2013	38631	58910	71.1	126.6	165.2	133.1	9.0	25.2
2014	32134	48065	69.2	113.9	104.3	127.3	8.8	26.3
2015	33674	50735	72.0	112.0	140.5	101.2	9.6	27.0
2016	39942	59763	72.9	140.7	155.4	165.1	10.2	24.0
2017	31496	49923	69.3	124.8	131.0	106.2	8.1	26.9
2018	36221	52371	72.5	114.1	119.6	99.4	10.6	25.9
2019	37168	60791	74.6	142.9	193.0	236.2	9.1	24.0
Average	33333	53110	71.0	122.4	148.3	140.9	8.5	25.3

the standard deviation value higher by a value of 2.85 than average had the fall (Fig. 5). During 2001-2019, 2008 and 2017 were the driest years (with precipitation anomalies of –3.7 and –3.9), and 2011 and 2019 which had precipitation anomalies of 4.94 and 3.6, respectively, have been the wettest years during the study period (Fig. 5).

In Fig. 6 the relationships between NDVI variations and winter precipitation, ET and LST in CSW during the study period are shown. There is a positive and significant correlation between NDVI, ET and LST in the study area for the time period of 2001-2019 (R = 0.46 and 0.55, respectively, p-value = 0.05). The relationship between NDVI and precipitation is positive, but not significant at a confidence level of 0.05. An assessment of the relationship between ET, LST and precipitation resulted in a positive and significant (R = 0.70, p-value = 0.05) correlation being found between ET and precipitation, but without any significant dependence of ET on LST being revealed. Therefore, it may be stated that the main factor controlling the dynamics of vegetation in the study area in the winter season, which is the coldest season (9.3°C), is LST. In the winter season, when precipitation is high enough, LST has a positive impact on ET. With the occurrence of low temperatures in the study area, the impact of precipitation on vegetation growth cannot be significant, because with low temperatures there is a low capacity for holding humidity, as well as the low temperatures themselves providing a limitation for vegetation growth (Kim *et al.,* 2014). For example, in 2005 LST was lower than usual (6.2°C), but precipitation was high, in fact

this year was the second wettest year during the studied period (after 2019), therefore, the vegetation coverage was lower than usual (32597 km²). On the other hand, in 2004 LST was 10°C higher than usual, and precipitation was equal to 133.1 mm (lower than the average value), but the vegetation coverage was 36931 km², significantly higher than usual (Fig. 6 and Table 3).

In Fig. 7, the relationships between NDVI variations and spring season precipitation, ET and LST in CSW during 2001-2019 are presented. A positive significant correlation between NDVI and ET and also precipitation in the study area during 2001-2019 (R = 0.86 and 0.55, respectively, with a p-value = 0.05), and a significant and negative correlation between NDVI and LST (R = –0.65, p-value = 0.05) may be observed. The correlation between ET and LST was negative and significant (R = –0.76, p-value = 0.05), while the correlation between ET and precipitation was positive and significant (R = 0.74, p-value = 0.05). From these correlations, it follows that in the spring season the main factor determining the vegetation dynamics in the study area is precipitation. In the spring season, which has moderate LST (25.29°C) and is the greenest period in the study area, when precipitation is high enough, vegetation coverage is extended and vice versa (Fig. 4). If precipitation in spring is higher than that which normally occurs in the study area in this period, LST's impact on vegetation growth is not significant, because LST in the spring season is already high enough (25.3°C) and is not a limiting factor for vegetation growth. For example, in 2003 and 2019, despite LST

Table 4. The relationship between vegetation coverage (VC) variations and summer and fall evapotranspiration (ET), precipitation and land surface temperature (LST) in the Caspian Sea Watershed during 2001-2019

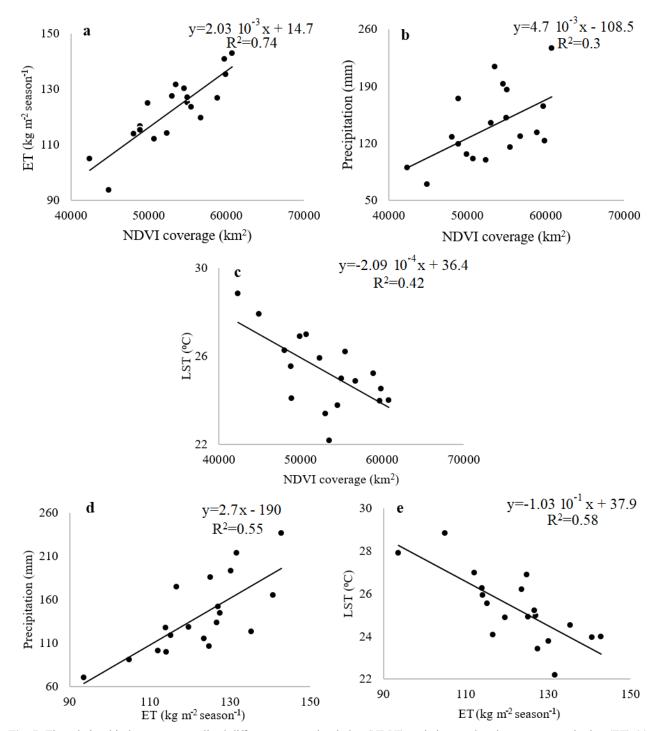| Year	Vegetation coverage (km²)		ET (kg m⁻² season⁻¹)		Precipitation (mm)		LST (°C)	
	Summer	Fall	Summer	Fall	Summer	Fall	Summer	Fall
2001	33517	29652	50.6	132.9	99.4	61.5	35.1	20.8
2002	38292	32062	94.1	145.7	111.2	58.1	37.2	22.9
2003	44106	34833	50.9	138.7	129.1	64.1	33.9	20.4
2004	40220	35437	70.4	148.9	120.8	63.9	34.7	20.6
2005	40254	37147	56.6	131.9	117.5	62.4	34.6	20.9
2006	36668	31016	20.4	140.6	95.1	62.4	36.8	20.4
2007	40686	34174	53.3	94.5	123.2	56.3	35.4	21.8
2008	34045	29353	34.0	120.2	97.2	62.0	36.0	21.0
2009	40438	31737	50.6	157.5	103.6	63.4	33.3	19.8
2010	40218	33772	38.9	74.8	96.2	54.1	36.5	23.6
2011	38857	34897	104.9	218.0	102.5	70.3	35.1	18.0
2012	42716	37965	94.1	145.7	119.4	68.3	34.9	21.8
2013	40947	33820	25.4	123.8	109.0	62.2	35.0	21.7
2014	37233	31338	48.7	147.1	95.5	65.7	36.5	19.6
2015	33674	35382	60.9	156.3	99.6	67.1	36.6	20.0
2016	40952	33633	51.3	134.7	121.8	62.3	35.7	20.8
2017	37549	33049	12.9	111.8	99.2	55.7	38.4	22.1
2018	38422	35570	30.4	131.7	86.4	65.6	37.1	21.2
2019	46916	35907	39.3	143.9	120.2	63.8	35.3	20.9
Average	39247	33723	52.0	136.8	107.7	62.6	35.7	21.0

Fig. 7. The relationship between normalized difference vegetation index (NDVI) variations and spring evapotranspiration (ET) (a), precipitation (b), and land surface temperature (LST) (c), and the relationship between spring ET with precipitation (d), spring ET with LST (e) in Caspian Sea Watershed during 2001-2019.

being lower than normal, and with precipitation higher than usual, the vegetation coverage was extended. On the other hand, a higher than normal LST accompanied by lower than usual precipitation due to their impact on ET (ET will be decreased because of low humidity), can become a limiting factor for vegetation growth and may result in a less green year, as was the case in 2001 and 2008 (Table 3).

In Fig. 8 the relationships between NDVI variations and summer season precipitation, ET and LST in CSW during 2001-2019 are shown. A positive significant correlation between NDVI and ET in the study area during 2001-2019 (R = 0.70, p-value = 0.05) and a negative significant correlation between NDVI and LST (R = –0.45, p-value = 0.05) was observed. The correlation between ET and LST
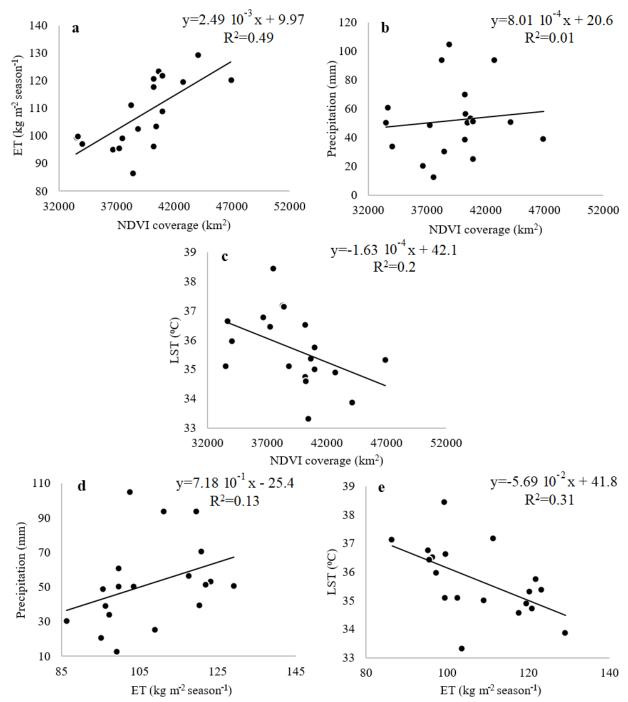
Fig. 8. The relationship between normalized difference vegetation Index (NDVI) variations and summer evapotranspiration (ET) (a) precipitation (b) and land surface temperature (LST) (c) and the relationship between summer ET with precipitation (d), summer ET with LST (e) in Caspian Sea Watershed during 2001-2019.

indicates that there is a negative and significant relationship between them (R = –0.56, p-value = 0.05), while the correlation between ET and precipitation is positive, but insignificant (R = 0.36). From these correlations, it follows that in the study area in the summer season the main factor that determines the vegetation dynamics is LST. The summer is the hottest season (35.69°C) in the study area, and when the LST value was lower than usual and precipitation was higher than usual, vegetation coverage was extended

(Fig. 5 and Table 4). In the case of precipitation higher than usual in the study area, the impact of LST on vegetation growth is very important, because very high LST causes a limitation in vegetation growth. For example, in 2002 and 2009 precipitation was equal to 111.2 and 103.6 mm, respectively, but the LST was 37.2 and 33.3°C, respectively, therefore despite 2002 being wetter than 2009, the vegetation coverage was higher in 2009 (Table 4).

Table 5. The relationship between vegetation coverage (VC) variations and fall Evapotranspiration (ET), precipitation (Precip) and land surface temperature (LST) in the Caspian Sea Watershed during 2001-2019

Model of vegetation coverage	R (regression coefficient)	R^2 (determination coefficient)	Multiple regression equations
Yearly	0.86	0.74	$VC_{yearly} = -33572 + 604.8\ ET_{yearly} - 7.9\ Precip_{yearly} + 982.4\ LST_{yearly}$
Winter	0.73	0.53	$VC_{winter} = -20486 + 594.2\ ET_{winter} + 6.4\ Precip_{winter} + 1259.6\ LST_{winter}$
Spring	0.88	0.77	$VC_{spring} = 22892 + 403.3\ ET_{spring} - 35.4\ Precip_{spring} - 559.4\ LST_{spring}$
Summer	0.72	0.52	$VC_{summer} = 30807 + 193.8\ ET_{summer} - 23.8\ Precip_{summer} - 313.8\ LST_{summer}$
Fall	0.55	0.30	$VC_{fall} = -26039 + 504.6\ ET_{fall} - 1.1\ Precip_{fall} + 1351.0\ LST_{fall}$

Fig. 9. The relationship between normalized difference vegetation index (NDVI) variations and fall evapotranspiration (ET) (a) precipitation (b) and land surface temperature (LST) (c) and the relationship between fall ET with precipitation (d), fall ET with LST (e) in Caspian Sea Watershed during 2001-2019.

In Fig. 9 the relationships between NDVI variations and fall season precipitation, ET and LST in CSW during 2001-2019 are presented. Insignificant and positive correlations between NDVI and ET and also precipitation (with R = 0.33 and 0.14, respectively) and no correlation between NDVI and LST were found in the study area during 2001-2019. The correlation between ET and LST indicates that there is a negative significant relationship between these factors (R = –0.78, p-value = 0.05), while the correlation between ET and precipitation is positive and significant (R = 0.82). From these correlations, it follows that the main factor determining the vegetation dynamics in the fall season in the study area is precipitation. The fall season is the moderate season (20.97°C) in the study area, and when precipitation is higher than usual, the vegetation coverage is extended. However, when precipitation is higher than usual and LST is lower than usual, it extends the vegetation coverage (as it was in, for example, in 2011) (Fig. 9 and Table 4).

For variations in vegetation coverage, multiple regression equations were calculated both for yearly and seasonal values (Table 5). These equations allow for an estimation of the projected value of vegetation coverage. The obtained multiple regression and determination coefficients indicate that ET, precipitation and LST explain about 75% of the yearly and spring vegetation coverage variation, and around 50% of its variation in the winter and summer.

DISCUSSION

In this study the variation in actual evapotranspiration (ET), precipitation and land surface temperature (LST) is characterized, and an assessment of the relationship between these climatic factors (ET, precipitation and LST) is performed for the period of 2001-2019 with vegetation dynamics in CSW . The study used MODIS images to obtain NDVI (MOD13Q1, 16 days, 250 m), LST (MOD11A2,
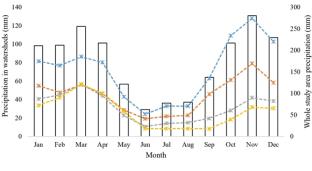

Fig. 10. The distribution of monthly precipitation in each watershed and the whole Caspian Sea Watershed including Lahijan-Noor Watershed (LNW), Haraz-Neka Watershed (HNW), Ghareso-Gorgan Watershed (GGW), and Atrak Watershed (AW) during 2001-2019.

eight days, 1 000 m), ET (MOD16A2GF, eight days, 500 m), and TRMM images (TRMM GPM_3IMERGM, 10 km) to calculate precipitation.

From the analysis of the interannual and inter-seasonal vegetation anomalies presented in this paper, it follows that substantial fluctuations occurred during 2001-2019 in the study area. The main findings of this study are as follows. The winter season with an average LST equal to 9.30°C is the coldest time period, the spring season with an LST equal to 25.29°C is mild, and the summer period is the hottest season (35.69°C) while fall is a moderate season (20.97°C) in the study area. The watersheds with the highest vegetation coverage simultaneously have the highest elevation, precipitation sums and lowest LST, and are located in the western part of the CSW watershed. When viewed from west to east the NDVI coverage, elevation, LST and precipitation decrease. The wettest (with the highest precipitation) season in the western watersheds (HNW and LNW) was the fall, in the eastern watersheds (GGW) – winter and spring, and in AW it was spring (Fig. 10).

LST plays the most important role in determining vegetation dynamics in cold seasons, while in the warm seasons both precipitation and LST are factors affecting the variation in vegetation in the study area. When a higher LST is recorded during a particular winter and fall it does not necessarily follow that this year will produce a vegetation coverage which is higher than average. LST can have a positive impact on ET when precipitation is high enough, but when LST is low, the impact of precipitation on vegetation coverage is not important, because with low LST there is also a low capacity for holding humidity (Ondier *et al.,* 2010; Rousta *et al.,* 2014). On the other hand, when high precipitation occurs in the spring and summer (especially in the spring season) it follows that a year with a positive anomaly of vegetation coverage in the study area is expected.

In the spring and summer seasons, if LST is higher than usual it is accompanied by precipitation lower than usual, ET is decreased because of low humidity (Allen *et al.,* 2007), and it becomes a limitation for vegetation growth, as it was in 2001 and 2008. When the usual precipitation is accompanied by LST which is higher (lower) than usual in these seasons, a year with lower (higher) vegetation coverage in the study area is observed (Schwingshackl *et al.,* 2017; Fan *et al.,* 2019). In the seasons with precipitation that is higher than average in the area, the impact of LST on vegetation growth was more pronounced. This is because LST in these seasons is very high, which in turn results in a much higher ET and causes soil moisture losses, which becomes a limitation for vegetation growth (Laio *et al.,* 2001; Karam *et al.,* 2003; Zhang *et al.,* 2019a, 2019b; Zhao T. *et al.,* 2021; Zhao X. *et al.,* 2020).

An anti-correlation between yearly NDVI and LST during the study period during 2001-2019 was observed, which resulted in positive NDVI anomalies for the years with negative LST anomalies. One exception was observed

for 2010, because in this year a positive anomaly in both the NDVI and LST was recorded. In order to shed light on this, a seasonal and after-seasonal assessment for the separate watersheds is required. In 2010, precipitation and LST in the western watersheds were higher than usual, which made them the greenest. Such conditions which resulted in favorable circumstances for vegetation growth affected the yearly NDVI anomaly and made it positive (Fig. 11).

CONCLUSIONS

1. Vegetation variations are surface phenomena, which may be a good indicator of climate change. These changes can be represented by an increase/decrease in temperature, precipitation, relative humidity, evapotranspiration, and other climatic variables. It was shown that climate change can have a great impact on vegetation variations in the Caspian Sea watersheds areas.

2. The present study attempted to identify and analyse the spatio-temporal variations in NDVI, ET, LST and precipitation in the whole Caspian Sea watersheds and its 4 sub-regions using remotely sensed satellite images. It was found that remote sensing images may be useful in monitoring the variations in vegetation in a humid area such as Caspian Sea Watersheds.

3. The indices retrieved from remote sensing for the period 2001-2019 indicated a considerable inter-seasonal and inter-annual variability, but no significant increasing/decreasing trends were found in the studied indices in Caspian Sea Watersheds during 2001-2019.

4. ET, precipitation and LST explain about 75% of the yearly and spring vegetation coverage variation in the Caspian Sea watershed areas.

5. Vegetation dynamics is a multi-aspect phenomenon that is affected by many factors including atmospheric patterns, atmospheric teleconnections and sea surface temperatures (especially in the Caspian Sea, which is the study area, the Mediterranean Sea and the Black Sea areas), the effects of human activities are also noteworthy. Also, the variations in the strength of Siberia's High pressure can have a great impact on the vegetation dynamics of Caspian Sea Watersheds, especially in the Caspian Hyrcanian forests. In future studies in the field of vegetation variations in the studied area, the factors mentioned above should be considered.

Conflict of interest: The authors declare that they have no conflict of interest.

REFERENCES

Alemu H., Senay G.B., Kaptue A.T., and Kovalskyy V., 2014. Evapotranspiration variability and its association with vegetation dynamics in the Nile Basin, 2002-2011. Remote Sens., 6, 5885-908, https://doi.org/10.3390/rs6075885

Allen R.G., Tasumi M., and Trezza R., 2007. Satellite-based energy balance for mapping evapotranspiration with internalized calibration (METRIC)-Model. J. Irrig. Drain. Eng., 133, 380-94, https://doi.org/10.1061/(ASCE)0733-9437(2007)133:4(380)

Bagherzadeh A., HoseiniA.V., and Totmaj L.H., 2020. The effects of climate change on normalized difference vegetation index (NDVI) in the Northeast of Iran. Mod. Earth Syst. Environ., 1-13, https://doi.org/10.1007/s40808-020-00724-x

Brutsaert W. and Stricker H., 1979. An advection-aridity approach to estimate actual regional evapotranspiration. Water Resour. Res., 15, 443-50, https://doi.org/10.1029/WR015i002p00443

Cai D., Fraedrich K., Sielmann F., Guan Y., Guo S., Zhang L., and Zhu X., 2014. Climate and vegetation: An ERA-Interim and GIMMS NDVI analysis. J. Clim., 27, 5111-18, https://doi.org/10.1175/JCLI-D-13-00674.1

Chanklan R., Suksut K., Chaiyakhan K., Kaoungku N., Kerdprasop K., and Kerdprasop N.. 2017. On applying regression and neural network to predict rainfall using satellite based index. In Proceedings of the International Multi Conference of Engineers and Computer Scientists, Hong kong, China.

Chao L., Zhang K., Wang J., Feng J., and Zhang M., 2021. A comprehensive evaluation of five evapotranspiration datasets based on ground and grace satellite observations: Implications for improvement of evapotranspiration retrieval algorithm. Remote Sens., 13, 2414, https://doi.org/10.3390/rs13122414

Chen Z., Liu Z., Yin L., and Zheng W., 2022. Statistical analysis of regional air temperature characteristics before and after dam construction. Urban Clim., 41, 101085, https://doi.org/10.1016/j.uclim.2022.101085

Cheng L., Xu Z., Wang D., and Cai X., 2011. Assessing interannual variability of evapotranspiration at the catchment scale using satellite-based evapotranspiration data sets. Water Resour. Res., 47, https://doi.org/10.1029/2011WR010636

Chuvieco E., Cocero D., Riano D., Martin P., Martınez-Vega J., De La Riva J., and Pérez F., 2004. Combining NDVI and surface temperature for the estimation of live fuel moisture content in forest fire danger rating. Remote Sens. Environ., 92, 322-31, https://doi.org/10.1016/j.rse.2004.01.019

Dhar S., Goswami S., Sarup J., and Matin S., 2020. Analysis of vegetation dynamics using remote sensing and GIS: a case study of Madhya Pradesh, India. Mod. Earth Sys. Environ., 7, 1039-1051, https://doi.org/10.1007/s40808-020-00998-1

Didan K., 2015. MOD13Q1 MODIS/Terra vegetation indices 16-day L3 global 250m SIN grid V006. NASA EOSDIS Land Processes DAAC.

Didan K., MunozA.B., Solano R., and Huete A., 2015. MODIS vegetation index user's guide (MOD13 series). University of Arizona: Vegetation Index and Phenology Lab, Version 3.00 (Collection 6), http://vip.arizona.edu/documents/MODIS/MODIS_VI_UsersGuide_June_2015_C6.pdf

Dutta D., Kundu A., Patel N., Saha S., and Siddiqui A., 2015. Assessment of agricultural drought in Rajasthan (India) using remote sensing derived Vegetation Condition Index (VCI) and Standardized Precipitation Index (SPI). Egypt. J. Remote Sens. Space Sci., 18, 53-63, https://doi.org/10.1016/j.ejrs.2015.03.006

Fan K., Zhang Q., V.P. Singh, Sun P., Song C., Zhu X., Yu H., and Shen Z., 2019. Spatiotemporal impact of soil moisture on air temperature across the Tibet Plateau. Sci. Total Environ., 649, 1338-1348, https://doi.org/10.1016/j.scitotenv.2018.08.399

Fayech D. and Tarhouni J., 2020. Climate variability and its effect on normalized difference vegetation index (NDVI) using remote sensing in semi-arid area. Mod. Earth Sys. Environ., 7, 1667-1682, https://doi.org/10.1007/s40808-020-00896-6

Fonge B.A., Tabot P.T., Bakia M.-A., and Awah C.C., 2019. Patterns of land-use change and current vegetation status in peri-urban forest reserves: the case of the Barombi Mbo Forest Reserve, Cameroon. Geol., Ecol. Landsc., 3, 104-13, https://doi.org/10.1080/24749508.2018.1508981

Geerken R., Zaitchik B., and Evans J., 2005. Classifying range-land vegetation type and coverage from NDVI time series using Fourier Filtered Cycle Similarity. Int. J. Remote Sens., 26, 5535-5554, https://doi.org/10.1080/01431160500300297

Ghafarian Malamiri H., Rousta I., Olafsson H., Zare H., and Zhang H., 2018. Gap-filling of MODIS time series Land Surface Temperature (LST) products using Singular Spectrum Analysis (SSA). Atmosphere, 9, 334, https://doi.org/10.3390/atmos9090334

Goward S.N., Markham B., Dye D.G., Dulaney W., and Yang J., 1991. Normalized difference vegetation index measurements from the Advanced Very High Resolution Radiometer. Remote Sens. Environ., 35, 257-77, https://doi.org/10.1016/0034-4257(91)90017-Z

Hadian F., Hosseini S.Z., and Seydhasani M., 2014. Monitoring vegetation changes using precipitation data and satellite images in northwest of Iran. Iran. J. Range Des. Res., 21, 756-767.

Huffman G., Stocker E., Bolvin D., Nelkin E., and Jackson T., 2019. "GPM IMERG final precipitation L3 half hourly 0.1 degree× 0.1 degree V06, Greenbelt, MD, Goddard Earth Sciences Data and Information Services Center (GES DISC)." In.

Jelínek Z., Kumhálová J., Chyba J., Wohlmuthová M., Madaras M., and Kumhála F., 2020. Landsat and Sentinel-2 images as a tool for the effective estimation of winter and spring cultivar growth and yield prediction in the Czech Republic. Int. Agrophys., 34(3), 391-406, https://doi.org/10.31545/intagr/126593

Karam F., Breidy J., Stephan C., and Rouphael J., 2003. Evapotranspiration, yield and water use efficiency of drip irrigated corn in the Bekaa Valley of Lebanon. Agric. Water Manag., 63, 125-37, https://doi.org/10.1016/S0378-3774(03)00179-3

Kim Y., Kimball J.S., Zhang K., Didan K., Velicogna I., and McDonald K.C., 2014. Attribution of divergent northern vegetation growth responses to lengthening non-frozen seasons using satellite optical-NIR and microwave remote sensing. Int. J. Remote Sens., 35, 3700-3721, https://doi.org/10.1080/01431161.2014.915595

Laio F., Porporato A., Fernandez-Illescas C., and Rodriguez-Iturbe I., 2001. Plants in water-controlled ecosystems: active role in hydrologic processes and response to water stress: IV. Discussion of real cases. Adv. Water Res., 24, 745-762, https://doi.org/10.1016/S0309-1708(01)00007-0

Lan Z., Zhao Y., Zhang J., Jiao R., Khan M.N., Sial T.A., and Si B., 2021. Long-term vegetation restoration increases deep soil carbon storage in the Northern Loess Plateau. Sci. Rep., 11, 1-11, https://doi.org/10.1038/s41598-021-93157-0

Lereboullet A.-L., Beltrando G., and Bardsley D.K., 2013. Socio-ecological adaptation to climate change: A comparative case study from the Mediterranean wine industry in France and Australia. Agric. Ecos. Environ., 164, 273-85, https://doi.org/10.1016/j.agee.2012.10.008

Loveland T.R., Zhu Z., Ohlen D.O., Brown J.F., Reed B.C., Yang L., 1999. An analysis of the IGBP global land-cover characterization process. Photogramm. Eng. Remote Sens., 65, 1021-1032, https://www.researchgate.net/profile/Jesslyn-Brown/publication/239665259_An_Analysis_of_IGBP_Global_Land-Cover_Characterization_Process/links/5553609e08ae980ca60853ae/An-Analysis-of-IGBP-Global-Land-Cover-Characterization-Process.pdf

Mansourmoghaddam M., Ghafarian Malamiri H.R., Rousta I., Olafsson H., and Zhang H., 2022a. Assessment of Palm Jumeirah Island's construction effects on the surrounding water quality and surface temperatures during 2001-2020. Water, 14, 634, https://doi.org/10.3390/w14040634

Mansourmoghaddam M., Rousta I., Zamani M.S., Mokhtari M.H., Karimi Firozjaei M., and Alavipanah S.K., 2022b. Investigating and modeling the effect of the composition and arrangement of the landscapes of Yazd City on the land surface temperature using machine learning and Landsat-8 and Sentinel-2 data. Iran. J. Remote Sens. GIS.

Mansourmoghaddam M., Rousta I., Zamani M., Mokhtari M.H., Karimi Firozjaei M., and Alavipanah S.K., 2021. Study and prediction of land surface temperature changes of Yazd city: Assessing the proximity and changes of land cover. J.. GIS RS for Natur. Res., 12, 1-27.

Martínez B. and Gilabert M.A., 2009. Vegetation dynamics from NDVI time series analysis using the wavelet transform. Remote Sens. Environ., 113, 1823-42, https://doi.org/10.1016/j.rse.2009.04.016

Miao R., Liu Y., Wu L., Wang D., Liu Y., Miao Y., Yang Z., Guo M., and Ma J., 2022. Effects of long-term grazing exclusion on plant and soil properties vary with position in dune systems in the Horqin Sandy Land. Catena, 209, 105860, https://doi.org/10.1016/j.catena.2021.105860

Moulin S., Kergoat L., Viovy N., and Dedieu G., 1997. Global-scale assessment of vegetation phenology using NOAA/AVHRR satellite measurements. J. Clim., 10, 1154-70, https://doi.org/10.1175/1520-0442(1997)010<1154:GSAOVP>2.0.CO;2

Oki T. and Kanae S., 2006. Global hydrological cycles and world water resources. Sci., 313, 1068-72, https://doi.org/10.1126/science.1128845

Olafsson H. and Rousta I., 2021. Influence of atmospheric patterns and North Atlantic Oscillation (NAO) on vegetation dynamics in Iceland using Remote Sensing. Eur. J. Remote Sens., 54, 351-63, https://doi.org/10.1080/22797254.2021.1931462

Ondier G.O., Siebenmorgen T.J., and Mauromoustakos A., 2010. Low-temperature, low-relative humidity drying of rough rice. J. Food Engin., 100, 545-50, https://doi.org/10.1016/j.jfoodeng.2010.05.004

Paraskevas C., Georgiou P., Ilias A., Panoras A., and Babajimopoulos C., 2013. Evapotranspiration and simulation of soil water movement in small area vegetation. Int. Agrophys., 27, 445-453, https://doi.org/10.2478/intag-2013-0015

Patel N., Chopra P., and Dadhwal V., 2007. Analyzing spatial patterns of meteorological drought using standardized precipitation index. Meteorol. Appl., 14, 329-336, https://doi.org/10.1002/met.33

Picoli M.C.A., Machado P.G., Duft D.G., Scarpare F.V., Corrêa S.T.R., Hernandes T.A.D., and Rocha J.V., 2019. Sugarcane drought detection through spectral indices derived modeling by remote-sensing techniques. Mod. Earth Sys. Environ., 5, 1679-1688, https://doi.org/10.1007/s40808-019-00619-6

Poorzady M. and Bakhtiari F., 2009. Spatial and temporal changes of Hyrcanian forest in Iran. iForest, 2, 198-206, https://doi.org/10.3832/ifor0515-002

Quaye-Ballard J.A., Okrah T.M., Andam-Akorful S.A., Awotwi A., Osei-Wusu W., Antwi T., and Tang X., 2020. Assessment of vegetation dynamics in Upper East Region of Ghana based on wavelet multi-resolution analysis. Mod.Earth Sys. Environ., 6, 1783-93, https://doi.org/10.1007/s40808-020-00789-8

Roerink G.J., Menenti M., Soepboer W., and Su Z., 2003. Assessment of climate impact on vegetation dynamics by using remote sensing. Phys. Chem. Earth, 28, 103-09, https://doi.org/10.1016/S1474-7065(03)00011-1

Rousta I., Doostkamian M., Taherian A.M., Haghighi E., Ghafarian Malamiri H.R., and Ólafsson H., 2017. Investigation of the spatio-temporal variations in atmosphere thickness pattern of Iran and the Middle East with special focus on precipitation in Iran. Climate, 5, 82, https://doi.org/10.3390/cli5040082

Rousta I., Javadizadeh F., Dargahian F., Ólafsson H., Shiri-Karimvandi A., Vahedinejad S.H., Doostkamian M., Monroy Vargas E.R., and Asadolahi A., 2018. Investigation of vorticity during prevalent winter precipitation in Iran. Adv. Meteorol., 2018, https://doi.org/10.1155/2018/6941501

Rousta I., Khosh Akhlagh F., Soltani M., and Modir Taheri Sh. S., 2014. "Assessment of blocking effects on rainfall in northwestern Iran." In COMECAP 2014, 127-32. Heraklion-Grecce: COMECAP.

Rousta I., Olafsson H., Moniruzzaman M., Ardö J., Zhang H., Mushore T.D., Shahin S., and Azim S., 2020a. The 2000-2017 drought risk assessment of the western and southwestern basins in Iran. Mod. Earth Sys. Environ., 6, 1201-1221, https://doi.org/10.1007/s40808-020-00751-8

Rousta I., Olafsson H., Moniruzzaman M., Zhang H., Liou Y.-A., Mushore T.D., and Gupta A., 2020b. Impacts of drought on vegetation assessed by vegetation indices and meteorological factors in Afghanistan. Remote Sens., 12, 2433, https://doi.org/10.3390/rs12152433

Rousta I., Olafsson H., Nasserzadeh M.H., Zhang H., Krzyszczak J., and Baranowski P., 2021. Dynamics of daytime land surface temperature (LST) variabilities in the Middle East countries during 2001-2018. Pure Appl. Geophys., 178, 2357-2377, https://doi.org/10.1007/s00024-021-02765-4

Running S.W., Mu Q., Zhao M., and Moreno A., 2019. MODIS global terrestrial evapotranspiration (ET) product (MOD16A2/A3 and year-end gap-filled MOD16A2GF/A3GF) NASA Earth Observing System MODIS land algorithm (For Collection 6).

Schwingshackl C., Hirschi M., and Seneviratne S.I., 2017. Quantifying spatiotemporal variations of soil moisture control on surface energy balance and near-surface air temperature. J. Clim., 30, 7105-24, https://doi.org/10.1175/JCLI-D-16-0727.1

Shahbazi F., Jafarzadeh A.A., Sarmadian F., Neyshabouri M., Oustan S., Anaya Romero M., Lojo M., and Rosa D.d.l., 2009. Climate change impact on land capability using MicroLEIS DSS, Int. Agrophys., 23(3), 277-286.

Shen G. and Wang R., 2001. Review of the application of vegetation remote sensing. J. Zhejiang Univ. - Agric. Life Sci., 27, 682-690.

Song K.-B., Baek Y.-S., Hong D.H., and Jang G., 2005. Short-term load forecasting for the holidays using fuzzy linear regression method. IEEE Trans. Power Syst., 20, 96-101, https://doi.org/10.1109/TPWRS.2004.835632

Tang Q., Vivoni E.R., Muñoz-Arriola F., and Lettenmaier D.P., 2012. Predictability of evapotranspiration patterns using remotely sensed vegetation dynamics during the North American monsoon. J. Hydrometeorol., 13, 103-121, https://doi.org/10.1175/JHM-D-11-032.1

Tavazohi E. and Nadoushan M.A., 2018. Assessment of drought in the Zayandehroud basin during 2000-2015 using NDDI and SPI indices. Fresenius Environ. Bull., 27, 2332-2340.

Telak L.J., Pereira P., and Bogunovic I., 2021. Soil degradation mitigation in continental climate in young vineyards planted in Stagnosols. Int. Agrophys., 35, 307-317, https://doi.org/10.31545/intagr/143268

Vilček J., Koco Š., Torma S., Lošák T., and Antonkiewicz J., 2019. Identifying soils for reduced tillage and no-till farming using GIS. Pol. J. Environ. Stud., 28(4), 2407-2413, https://doi.org/10.15244/pjoes/90787

Wan Z., Hook S., and Hulley G., 2015. MOD11 L2 MODIS/terra land surface temperature/emissivity 5-Min L2 Swath 1 km V006. NASA EOSDIS Land Processes DAAC.

Zandbergen P., 2008. Applications of shuttle radar topography mission elevation data. Geogr. Compass, 2, 1404-1431, https://doi.org/10.1111/j.1749-8198.2008.00154.x

Zhan S., Song C., Wang J., Sheng Y., and Quan J., 2019. A global assessment of terrestrial evapotranspiration increase due to surface water area change. Earths Future, 7(3), 266-282, https://doi.org/10.1029/2018EF001066

Zhang K., Ali A., Antonarakis A., Moghaddam M., Saatchi S., Tabatabaeenejad A., Chen R., Jaruwatanadilok S., Cuenca R., and Crow W.T., 2019a. The sensitivity of North American terrestrial carbon fluxes to spatial and temporal variation in soil moisture: An analysis using radar-derived estimates of root-zone soil moisture. J. Geophys. Res. Biogeosci., 124(11), 3208-3231, https://doi.org/10.1029/2018JG004589

Zhang K., Chao L.-j., Wang Q.-q., Huang Y.-c., Liu R.-h., Hong Y., Tu Y., Qu W., and Ye J.-y., 2019b. Using multi-satellite microwave remote sensing observations for retrieval of daily surface soil moisture across China. Water Sci. Eng., 12(2), 85-97, https://doi.org/10.1016/j.wse.2019.06.001

Zhang K., Wang S., Bao H., and Zhao X., 2019c. Characteristics and influencing factors of rainfall-induced landslide and debris flow hazards in Shaanxi Province, China. Nat. Hazards Earth Syst. Sci., 19, 93-105, https://doi.org/10.5194/nhess-19-93-2019

Zhang W., Liu B., and Wu J., 2001. Monitoring of plant coverage of plots by visual estimation and overhead photograph. Bull. Soil Water Conserv., 21, 60-63.

Zhang X., 2020. The optimization of spatial art pattern of vegetation landscape in the Bay Area. J. Coastal Res., 103, 1051-1055, https://doi.org/10.2112/SI103-219.1

Zhao T., Shi J., Entekhabi D., Jackson T.J., Hu L., Peng Z., Yao P., Li S., and Kang C.S., 2021. Retrievals of soil moisture and vegetation optical depth using a multi-channel collaborative algorithm. Remote Sens. Environ., 257, 112321, https://doi.org/10.1016/j.rse.2021.112321

Zhao T., Shi J., Lv L., Xu H., Chen D., Cui Q., Jackson T.J., Yan G., Jia L., and Chen L., 2020. Soil moisture experiment in the Luan River supporting new satellite mission opportunities. Remote Sens. Environ., 240, 111680, https://doi.org/10.1016/j.rse.2020.111680

Zhao X., Xia H., Pan L., Song H., Niu W., Wang R., Li R., Bian X., Guo Y., and Qin Y., 2021. Drought monitoring over Yellow River basin from 2003-2019 using reconstructed MODIS land surface temperature in Google Earth Engine. Remote Sens., 13, 3748, https://doi.org/10.3390/rs13183748

Zhong L., Ma Y., Salama M.S., and Su Z., 2010. Assessment of vegetation dynamics and their response to variations in precipitation and temperature in the Tibetan Plateau. Clim. Change, 103, 519-535, https://doi.org/10.1007/s10584-009-9787-8